Finite-Volume and Finite-Element Hybrid Technique for the Calculation of Complex Heat Exchangers by Semiexplicit Method for Wall Temperature Linked Equations (SEWTLE)

Pietro Asinari

7th January 2004

Institutional Affiliation:
Dipartimento di Energetica, Politecnico di Torino
Corso Duca degli Abruzzi 24, Zip Code 10129, Torino, Italy
Tel. +39-011-564-4413, Telefax. +39-011-564-4499
E-mail: pietro.asinari@polito.it

Abbreviated Title:
FVM-FEM Technique for Complex Heat Exchangers

Abstract

An analysis has been performed about the discretization of governing equations for complex heat exchangers. The grid generation and the cell discretization have been discussed separately, to investigate the possibilities for improving the accuracy of description. A finite-volume and finite-element hybrid technique, which is compatible with semiexplicit method for wall temperature linked equations (SEWTLE), is proposed. This technique produces accurate temperature profile within the cell and reduces the number of grid points. Advantages, drawbacks and application strategies are reported.

Nomenclature

a, b	dimensionless constants	S	specific thermal source (W/m^3)
A	heat transfer surface (m^2)	T	temperature (K)
Bi	Biot number	P	generic point (x, y, z)
c_p	specific heat (J/kgK)	$\mathbf{u}$	velocity vector (m/s)
C_i	dimensional constants (K)	$[\mathbf{U}]$	matrix multipling upstream
$[\mathbf{F}]$	matrix multipling fluid		fluid temperature vector (W/K)
	temperature vector (W/K)	V	volume (m^3)
G	mass flow rate (kg/s)	x, y, z	spatial coordinates (m)
h	specific entalphy (J/kg)	x_0	fin length (m)
J	specific thermal flux (W/m^2)	z_0	fin height (m)
k	thermal conductivity (W/mK)	$\bar{Z}$	set of index vectors
$\mathbf{n}$	unit vector	$[\mathbf{W}]$	matrix multipling wall
N	natural number		temperature vector (W/K)
s	wall thickness (m)		

Greek symbols

α	heat transfer coefficient (W/m^2K)	σ	border surface of
δx	step of fin discretization (m)		three-dimensional discretized domain
Φ	thermal flux (W)	Σ	border surface of
ω	three-dimensional discretized domain		three-dimensional domain
Ω	three-dimensional domain	θ	temperature difference (K)
ρ	density (kg/m^3)		

Subscripts and superscripts

c	calculation	k	heat conduction
C	thermal capacity	e	EBS elementary surface index
D	downstream	h	HBS elementary surface index
E	FEM	l	EBS cell index
EBS	heterogeneous	m	HBS cell index
	boundary sub-domain	N,S,W,E	north, sud, west, east
EN	environment	t	top
f	fluid	U	upstream
fp	fluid path	V	FVM
HBS	homogeneous	w	wall
	boundary sub-domain	XBS	intersected
i	fluid index		boundary sub-domain
j	fluid cell index		

Operators and convention

$\nabla_2(X)$	two-dimensional	Δ	differential portion
	gradient of X	$\mathbf{X}$	vector
$\nabla_3(X)$	three-dimensional	$[\mathbf{X}]$	matrix
	gradient of X	$\bar{X}$	set
$\nabla \bullet (\mathbf{X})$	divergence of vector $\mathbf{X}$		

1 Introduction

Heat exchangers occupy a unique position among thermal engineering applications because they are widely spread in many industrial fields covering all possible physical sizes and constitute the key elements to determine the thermal system performances.

The first theoretical efforts on the subject produced analytical treatment of idealized devices. These works produced a range of global methods, like the Logarithmic Mean Temperature Difference (LMTD) and the Effectiveness-Number of Transfer Units (ϵ-NTU) [1]. However, global methods are based on a number of assumptions (i.e. steady flow, single-phase flow, constant thermo-physical properties, constant heat transfer coefficients, negligible longitudinal wall conduction and so on), which are hardly met in practical applications. In particular, real heat exchangers often involve two-phase flow processes, air dehumidification and variable fluid properties.

In addition, the interest for more sophisticated heat exchangers is increasing because of the need for better overall efficiency and decrease in size and weight. In all varieties of powered vehicles from automobiles to spacecrafts, the trend for small-size and lightweight heat exchangers has stimulated the development of heat transfer surfaces much more compact than in classical devices [2]. In compact devices, some effects neglected by classical theory can influence the overall behavior. Obviously, a rationally optimised heat exchanger design and the definition of new surfaces of better characteristics require the development of reliable tools.

The need for detailed analysis of practical situations demands the employment of computational techniques, which allow a close representation of reality. Nowadays, a lot of general-purpose codes for Computational Fluid Dynamics (CFD) are available and can be applied to heat exchangers: for instance, the FLUENT© code [3] or the FIDAP© code [4], both commercial ones. Despite its versatility, a general-purpose code can be characterized by some drawbacks if compared with an application-oriented one. In particular, a general purpose code can require large meshes and unacceptable conputational time to describe specific details of complex applications. Furthermore, some parametric studies involve geometric characteristics, which need frequent re-meshing and heavy post-processing. Finally, general-purpose codes are not usually suitable to produce a stand-alone module for the analysis of interactions between a heat exchanger and the whole system: this goal can only be achieved by modifying iteratively the boundary conditions of the problem.

On the other hand, the application-oriented codes for heat exchangers apply discretization techniques which, although general in nature, have been fitted to the analysis of a particular effect. Some examples can be found in literature which consider longitudinal heat conduction [5, 6], nonuniformity of the inlet fluid flow [7] or the mutual interaction between previous effects [8, 9]. Only a few studies have been devoted to discussing and developing a general numerical formulation. Recently, a general numerical approach for heat exchangers, called semiexplicit method for wall temperature linked equations SEWTLE, has been proposed [10]. The method decouples the calculation of wall temperature field from that of fluid temperature field and computes the final solution by means of an iterative procedure which is controlled by continuity of heat flow between hot-side thermal flux and cold-side one. Since this method employs the thermal balance as convergence check, a conservative scheme for the discretization of involved equations, as the Finite Volume Method (FVM), represents the most natural choice and it was included in the original paper.

In compact heat exchangers, some configurations exist for which the FVM is not

suitable with regard to wall domain discretization. In these applications, the original formulation of SEWTLE technique based on FVM is not useful. This work aims at showing that the SEWTLE approach is more general than original formulation suggests because it can consider different numerical schemes, allowing more flexible descriptions.

2 Problem definition

Generally, the equations describing a heat exchanger are defined on a computational domain composed by the fluid region and surrounding wall.

The fluid region can be divided into a set of one-dimensional streams, following the flow field. The possibility of a mixing region, which receives some fluid streams and produces average conditions, can be easily included. In this case, each fluid stream is conceptually identical to each other and there is no need to give up the FVM, which represents the easiest choice for the discretization of fluid equations.

On the other hand, the wall domain does not demonstrate the same situation. In fact, a distinction always exists among the separating walls which constitute the heat exchanger: some of them are in direct contact with fluids of different nature, while some others are in contact with fluids of the same nature. Referring to convection phenomenon, the first class of separating walls constitutes the heterogeneous boundary sub-domain (EBS), while the last class constitutes the homogeneous boundary sub-domain (HBS): for instance, the case of crossflow plate-fin heat exchanger is reported in Figure 1*a*. The EBS is the physical substratum which makes the heat transfer possible between different fluids (hot-side and cold-side) while the HBS is an optional extension of separating wall, which has been introduced for enhancing heat transfer surfaces. For crossflow plate-fin heat exchangers, the EBS is constituted by surfaces oriented in fluid directions while the HBS couples the previous surfaces by transverse fins. Finally, the EBS is usually characterized by convective fluxes due to strong temperature gradients while the HBS involves small non homogenities due to adjacent fluid paths. Since the numerical discretization must be matched on the physical behavior of the considered portion, the distinction between EBS and HBS suggests choosing different schemes, if the above discrepancies are considerable.

The difference between the discussed sub-domains becomes evident when a low heat transfer coefficient characterizes one of the fluids. Within this set of applications, the cross-flow plate-fin compact heat exchangers with microchannels, used in gas cooling applications, portray the most extreme example [11]. In this case, the fins for penalized fluid are increased while the other ones constitute the vertical separating walls, which identify the microchannels (Figure 1*b*). The fin surface is mainly responsible for whole device behavior. When one of the fin roots is characterized by inverse thermal flux directed towards heated wall, the fin efficiency is drastically reduced and a thermal bridge exists. The importance of thermal bridges has been shown analytically in simplified configurations [12] and by means of detailed simulations for a particular fin surface [13]. Unfortunately thermal bridges are influenced by the topology of fluid circuits because they contribute to determine the final temperature distribution. Detailed simulations for whole HBS are not practicable and, on the other hand, a reduction of unknown variables must be performed by preserving the physical meaning. Thermal bridges for compact heat exchangers with microchannels represent a good opportunity to investigate the possibilities for optimisation of wall domain discretization within the framework of the SEWTLE technique.

3 Governing equations

Let us consider again the compact heat exchanger shown in Figure 1*b*. The following considerations can be easily extended to different flow arrangements and geometry.

With a purpose to identify the sub-domains which constitute the calculation domain Ω_c, some definitions are introduced for volumes, as shown in Figure 1*c*.

$$\begin{aligned} \Omega_c &\doteq \Omega_w \cup \Omega_f \\ \Omega_w &\doteq \Omega_{EBS} \cup \Omega_{HBS} \\ \Omega_f &\doteq \bigcup_{i=1}^{N_{fp}} \Omega_i \end{aligned} \tag{1}$$

Where Ω_w is the wall domain, which can be divided in Ω_{EBS} for EBS and Ω_{HBS} for HBS, while Ω_f is the fluid domain, which can be divided into N_{fp} sub-domains Ω_i for each fluid.

Additional definitions are introduced for surfaces, as shown in Figure 1*c*.

$$\begin{aligned} \Sigma_f &\doteq \bigcup_{i=1}^{N_{fp}} \Sigma_i \\ \Sigma_w &\doteq \Sigma_{EN} \cup \Sigma_f \\ \Sigma_i &\doteq \Sigma_i^{EBS} \cup \Sigma_i^{HBS} \end{aligned} \tag{2}$$

Where Σ_{EN} is the portion of wall surface which is in contact with the external environment.

For steady conditions and single-phase flow, the energy conservation equations can be written for each sub-domain.

$$P \in \Omega_i \quad ; \quad \int_{\Sigma_i} (\rho_i h_i \mathbf{u_i}) \bullet \mathbf{n} dA = \int_{\Sigma_i} \mathbf{J_i} \bullet \mathbf{n} dA + \int_{\Omega_i} S_i dV \tag{3}$$

$$P \in \Omega_w \quad ; \quad \int_{\Omega_w} \nabla_3 \bullet (k_w \nabla_3 T_w) dV = -\sum_{i=1}^{N_{fp}} \int_{\Sigma_i} \mathbf{J_i} \bullet \mathbf{n} dA - \int_{\Sigma_{EN}} \mathbf{J_{EN}} \bullet \mathbf{n} dA = 0 \tag{4}$$

where

$$\mathbf{J_i} \doteq - k_i \left[\nabla_3 T_i\right]_{\Sigma_i}$$

where N_{fp} is the number of fluid paths in the heat exchanger. The vector $\mathbf{n}$ must be considered positive if leaving from wall domain or from calculation domain.

Since no energy generation has been supposed inside the wall, the overall thermal balance involves only the fluid paths.

$$\sum_{i=1}^{N_{fp}} \left[\int_{\Sigma_i} (\rho_i h_i \mathbf{u_i}) \bullet \mathbf{n} dA - \int_{\Omega_i} S_i dV \right] + \int_{\Sigma_{EN}} \mathbf{J_{EN}} \bullet \mathbf{n} dA = 0 \tag{5}$$

In addition to the energy conservation equation, the momentum conservation and the continuity equations must be considered to provide the full Navier-Stokes model needed to calculate pressure and velocity. Anyway, some simplifying hypotheses can be introduced.

If the fluid is incompressible, the energy equation is decoupled from the system and can be solved independently. If the fluid flow is assumed one-dimensional, it is not possible to calculate the cross flow gradients involved in convective fluxes, which must be calculated by means of heat transfer coefficients. Finally, if the viscous dissipation can be neglected, the heat generation in the energy conservation equations can be removed.

$$P \in \Omega_i \quad ; \quad \int_{A_U+A_D} (\rho_i h_i \mathbf{u_i}) \bullet \mathbf{n} dA = \int_{\Sigma_i} \mathbf{J_i} \bullet \mathbf{n} dA \tag{6}$$

where

$$\mathbf{J_i} \doteq \alpha_i (T_w - T_i)\mathbf{n}$$

These equations are enough to show the effects of numerical discretization schemes.

4 Boundary conditions

Usually at the fluid inlet, Dirichlet-type conditions are imposed because the fluid states depend on the behavior of the upstream devices. On the other hand, a Neumann-type condition is imposed on the portion of the wall surface which is in contact with the external environment, because the heat exchangers are usually well insulated.

$$\forall i : 1 \leq i \leq N_{fp} \quad ; \quad T_i^U = \text{cost} \quad ; \quad \int_{\Sigma_{EN}} \mathbf{J_{EN}} \bullet \mathbf{n} dA = 0 \tag{7}$$

The resulting system of equations is composed by a sub-system of ordinary differential equations (ODEs), one for each fluid path, with Dirichlet-type boundary conditions and a partial differential equation (PDE) for the separating wall with Neumann-type boundary condition. When the longitudinal conduction is negligible and the convective heat transfer coefficients do not depend on the wall temperature, the last PDE becomes a linear condition for wall temperature which can be expressed as function of the neighbor fluid temperatures. In this way, the system can be reduced to a pure system of ODEs. Unfortunately, in some applications [11], the last hypothesis does not hold and it is useful to include the calculation of wall temperature in the numerical procedure [10]. Since this calculation is time-consuming, we need to choose properly the cell discretization and the numerical scheme for the wall.

5 Mesh definition

The mesh construction can be divided in two steps.

The first step replaces the continuos information contained in the exact solution of differential equations with discrete values at a finite number of locations in the calculation domain (*grid* points). Obviously, the best grid choice depends on the nature of the differential equations. For this reason, in Figure 2, the grid points for wall domain governed by PDE (square markers) have been separated from the grid points for a generic fluid sub-domain governed by ODE (arrow markers). For the accuracy of the numerical results, the relative displacement between wall and fluid grid must be discussed. Three cases are considered: longitudinal configuration (Figure 2*a*); transverse configuration (Figure 2*b*) and diagonal configuration (Figure 2*c*). The longitudinal configuration shows an important drawback because the wall temperature at the intersection between the general portion for EBS and the corresponding one for HBS is not considered directly

and must be evaluated by interpolation. In practical applications, this means that the longitudinal configuration is not suitable for studying the behavior of fins because it does not consider the fin root temperatures. Between two consecutive fluid grid points (arrow markers), the temperature profile inside the portion of heat transfer surface must be approximated by means of wall grid points (square markers). If we compare the ratios between wall points and fluid ones within a projection of generic fluid cell (Figure $2a$, $2b$ and $2c$), we find that the longitudinal configuration is the most penalized (1w/2f), followed by the diagonal one (2w/2f), while the transverse configuration is the most convenient (4w/2f). Although the decoupling between fluid and wall conditions increases the computational time, the transverse configuration will be adopted in the following.

The second step of the mesh definition is constituted by *cell* discretization, i.e. the subdivision of the calculation domain in suitable control volumes. Since each numerical scheme is characterized by preferable distribution of the grid points within the elementary control volume, the cell discretization arises from the choice of numerical scheme. The discussion about this choice has been split among the different parts of the calculation domain, as to demonstrate that the utilization of different numerical schemes is possible within the framework of the same grid configuration.

5.1 Discretization equations for Ω_f

The fluid paths are governed by ODEs characterized by first-order spatial derivative as main term. In this case, the Finite Volume Method (FVM) is the most natural choice and the use of a grid point at the fluid inlet and another one at the fluid outlet of the control volume is recommended. In this way, the first derivative can be efficiently approximated by the corresponding finite-difference expression linking the well-defined values of the variable at both ends [14].

If the fluid grid points are located at the edges of control volume, the number of the fluid cells N_i and their distribution are strictly tied to the grid spatial density. Inside each control volume, a distinction can be made between the surfaces belonging to different sub-domains (EBS or HBS).

Let us introduce the discretization definitions for surfaces.

$$\Sigma_i \doteq \bigcup_{j=1}^{N_i} \Delta(\Sigma_i)_j \tag{8}$$

Taking into account this discretization and applying an up-wind technique, the Eq. (6) produces N_f algebraic conditions for fluid.

$$\begin{aligned} \forall i,j \quad &: \quad 1 \leq i \leq N_{fp} \quad ; \quad 1 \leq j \leq N_i \\ G_i c_p (T_i^j - T_i^{j-1}) \quad &= \quad \int_{\Delta(\Sigma_i^{EBS})_j} \mathbf{J_{i,j}} \bullet \mathbf{n} dA + \int_{\Delta(\Sigma_i^{HBS})_j} \mathbf{J_{i,j}} \bullet \mathbf{n} dA \end{aligned} \tag{9}$$

where

$$\forall i : 1 \leq i \leq N_{fp} \quad ; \quad T_i^0 = T_i^U = \text{cost} \quad ; \quad N_f = \sum_{i=1}^{N_{fp}} N_i$$

The previous integrals are expressed as the sum of a finite number of terms, which represent the convective thermal fluxes exchanged through elementary surfaces. For

clarifying this subdivision, two elementary surfaces are shown in Figure $2d$, one for each wall sub-domain. Within each fluid cell, the identification of an elementary surface can be done by a local index which depends on the considered wall sub-domain (e for EBS and h for HBS).

$$\begin{aligned} \Delta(\Sigma_i^{EBS})_j &\doteq \bigcup_{e=1}^{8} \Delta(\Sigma_i^{EBS})_{j,e} \\ \Delta(\Sigma_i^{HBS})_j &\doteq \bigcup_{h=1}^{4} \Delta(\Sigma_i^{HBS})_{j,h} \end{aligned} \tag{10}$$

In this way, the discretization equations for fluid reduce to final form.

$$\begin{aligned} \forall i,j \quad &: \quad 1 \le i \le N_{fp} \quad ; \quad 1 \le j \le N_i \\ G_i c_p (T_i^j - T_i^{j-1}) &= \sum_{e=1}^{8} \Delta\Phi_{EBS}^{i,j,e} + \sum_{h=1}^{4} \Delta\Phi_{HBS}^{i,j,h} \end{aligned} \tag{11}$$

where

$$\begin{aligned} \Delta\Phi_{EBS}^{i,j,e} &\doteq \int_{\Delta(\Sigma_i^{EBS})_{j,e}} \mathbf{J_{i,j}} \bullet \mathbf{n} dA \\ \Delta\Phi_{HBS}^{i,j,h} &\doteq \int_{\Delta(\Sigma_i^{HBS})_{j,h}} \mathbf{J_{i,j}} \bullet \mathbf{n} dA \end{aligned} \tag{12}$$

These equations involve the calculation of thermal fluxes which must be consistent with the profile assumptions for both fluid and wall.

5.2 Discretization equations for Ω_{EBS}

Since the wall domain has been subdivided into two sub-domains, the splitting up of the wall grid points between them is not trivial. Consistent with the purpose to reduce the computational effort for HBS, all the wall grid points are supposed as belonging to EBS. In this way, in the resulting algebraic system there will be no equation which prescribes explicitly the energy conservation for HBS. The last condition will be considered implicitly when deriving the thermal flux expressions.

Before proceeding with discretization, the governing equations for wall sub-domains are derived, such as to express the effect of thermal coupling. The Eq. (4) can be split into two equations, one for each sub-domain.

$$P \in \Omega_{EBS} \quad ; \quad \int_{\Omega_{EBS}} \nabla_3 \bullet (k_w \nabla_3 T_w) dV = -\sum_{i=1}^{N_{fp}} \int_{\Sigma_{EBS}} \mathbf{J_i} \bullet \mathbf{n} dA + \Phi_{XBS} = 0 \tag{13}$$

$$P \in \Omega_{HBS} \quad ; \quad \int_{\Omega_{HBS}} \nabla_3 \bullet (k_w \nabla_3 T_w) dV = -\sum_{i=1}^{N_{fp}} \int_{\Sigma_{HBS}} \mathbf{J_i} \bullet \mathbf{n} dA - \Phi_{XBS} = 0 \tag{14}$$

where

$$\Phi_{XBS} = -\int_{\Sigma_{EBS}\cap\Sigma_{HBS}} k_w \nabla_3 T_w \bullet \mathbf{n_w} dA$$

The vector $\mathbf{n_w}$ must be considered positive if leaving from HBS and, consequently, entering into EBS. The first equation will be employed to determine the discretization conditions for wall grid points, while the last one will be involved in the definition of flux Φ_{XBS} exchanged between HBS and EBS.

Also in this case the FVM is recommended. A central control volume with a value of temperature defined at its center is adopted because it represents the most suitable configuration to evaluate second-order partial spatial derivatives. With the transverse grid configuration, some care must be taken to define half-volumes at the edge of the plates, such as to satisfy properly the boundary conditions [14]. The ambiguity due to the definition of wall temperatures at the fluid grid locations can be easily overcome by interpolation among the values in EBS.

If the wall grid point is located at the center of control volume, the cell discretization is completely defined (Figure 3a). The EBS can be subdivided into N_w control volumes.

$$\Omega_{EBS} = \sum_{l=1}^{N_w} \omega_{EBS}^l \tag{15}$$

Taking into account this discretization, the Eq. (13) produces N_w algebraic conditions for wall.

$$\begin{aligned} \forall l \quad &: \quad 1 \le l \le N_w \\ \int_{\sigma_{EBS}^l} \nabla_2 \bullet (k_w \nabla_2 T_w) s dA \quad &= \quad \Delta\Phi_{EBS}^l - \Delta\Phi_{XBS}^l \end{aligned} \tag{16}$$

where

$$\Delta\Phi_{EBS}^l = \sum_{i=1}^{N_{fp}} \int_{\sigma_{EBS}^l} \mathbf{J_i} \bullet \mathbf{n} dA$$

$$\Delta\Phi_{XBS}^l = -\int_{\sigma_{EBS}^l\cap\Sigma_{HBS}} k_w \frac{\partial T_w}{\partial z} \mathbf{n_z} \bullet \mathbf{n_w} dA$$

$\mathbf{n_z}$ is the unit vector of z-axis. Remembering the definitions expressed by Eqs. (12) and considering separately the contribution of each elementary surface to exchanged flux $\Delta\Phi_{XBS}^l$, the discretization equations for wall reduce to final form.

$$\begin{aligned} \forall l \quad &: \quad 1 \le l \le N_w \\ \int_{\sigma_{EBS}^l} \nabla_2 \bullet (k_w \nabla_2 T_w) s dA \quad &= \quad \sum_{(i,j,e)\in\bar{Z}_{EBS}^l} \left[\Delta\Phi_{EBS}^{i,j,e} - \Delta\Phi_{XBS}^{i,j,e}\right] \end{aligned} \tag{17}$$

where

$$\bar{Z}_{EBS}^l = \left\{\forall (i,j,e) : \Delta(\Sigma_i^{EBS})_{j,e} \subset \sigma_{EBS}^l\right\}$$

The congruence between the wall-side and the fluid-side heat transfer calculations can be easily verified, taking into account the following equivalence.

$$\sum_{l=1}^{N_w} \left[\sum_{(i,j,e)\in\bar{Z}_{EBS}^l} \Delta\Phi_{EBS}^{i,j,e}\right] = \sum_{i=1}^{N_{fp}} \sum_{j=1}^{N_i} \sum_{e=1}^{8} \Delta\Phi_{EBS}^{i,j,e} \tag{18}$$

5.3 Discretization equations for Ω_{HBS}

Although the governing equation is the same one considered previously for EBS, the choice of numerical approach must guarantee a physical meaningful description by applying only fin root temperatures. Within the set of integral formulations, two possibilities are suitable to discretize governing equations for HBS: *subdomain approach*, which is the basis of FVM, and *variational approach*, which is the basis of Finite Element Method (FEM) for problems which do not involve first-derivative terms [15].

The subdomain approach is a particular case of weighted residual formulation, where each weighting function is selected as unit over a specific portion of the calculation domain. Since the integral form of the energy conservation equation can be expressed in terms of thermal fluxes, the FVM applied to conduction problems must ensure the continuity of first-order partial spatial derivative at the border of adjacent volumes. A central control volume with a value of temperature defined at its center represents the easiest way to reach this goal.

The variational approach involves a functional which must be minimized over each discretization element according to the calculus of variations. The FEM considers trial temperature profiles which are continuous piecewise smooth functions and identifies among them the approximate solution which gives the minimum value of the functional. A surrounded element with values of the temperature defined at the border represents the easiest choice.

In our case, the discretization cell for generic fin should be characterized by coherent description of thermal fluxes due to longitudinal conduction and by detailed temperature profile in transverse direction. As it will be clearer in the following, it is suitable to locate the temperature values at the middle of root edges, as shown in Figure 3*b*. The HBS can be divided into N_{HBS} elements.

$$\Omega_{HBS} = \sum_{m=1}^{N_{HBS}} \omega_{HBS}^{m} \tag{19}$$

Taking into account this discretization and remembering the definitions for thermal fluxes due to convection, the Eq. (14) can be modified.

$$\begin{aligned} &\forall m : 1 \leq m \leq N_{HBS} \\ &\int_{\sigma_{HBS}^{m}} \left[s\nabla_2 \bullet (k_w \nabla_2 T_w) - \sum_{i=1}^{N_{fp}} \alpha_i (T_w - T_i) \right] dA = 0 \end{aligned} \tag{20}$$

Assuming the thermal conductivity as temperature invariant, the resolution of the previous equation can be considered equivalent to the minimization of the following functional.

$$\Pi = \int_{\sigma_{HBS}^{m}} \left[(\nabla_2 T_w) \bullet (\nabla_2 T_w) + \sum_{i=1}^{N_{fp}} \frac{\alpha_i}{k_w s} (T_w - T_i)^2 \right] dA \tag{21}$$

Let us apply the Euler-Ostrogradskij equation [16].

$$P \in \sigma_{HBS}^{m} \quad ; \quad \frac{\partial^2 \theta}{\partial x^2} + \frac{\partial^2 \theta}{\partial z^2} = \frac{Bi}{z_0^2} \theta \tag{22}$$

where

$$Bi = z_0^2 \frac{\sum_{i=1}^{N_{fp}} \alpha_i}{k_w s} \quad ; \quad \theta = T_w - \frac{\sum_{i=1}^{N_{fp}} \alpha_i T_i}{\sum_{i=1}^{N_{fp}} \alpha_i}$$

The solution of the Euler-Ostrogradskij equation is the temperature profile which gives the minimum value of the functional (21). Assuming constant fluid temperatures for the considered element, an analytical solution can be found according to the classical theory for extended surface heat transfer [17].

$$\theta(x,z) = C_1 \exp\left(\sqrt{Bi}\,\frac{x}{z_0}\right) + C_2 \exp\left(-\sqrt{Bi}\,\frac{x}{z_0}\right) + C_3 \exp\left(\sqrt{Bi}\,\frac{z}{z_0}\right) + C_4 \exp\left(-\sqrt{Bi}\,\frac{z}{z_0}\right) \tag{23}$$

The most natural choice for HBS element is the surrounded quadratic element shown in Figure ($3b$). This is equivalent to consider four Dirichlet conditions for determining constants C_i. Since unfortunately these conditions are not linearly independent for function (23), they do not allow defining uniquely the set of constants. The basic idea is to "shift" or "move" the element, as shown in Figure ($3b$). In this case, two boundary conditions belong to Dirichlet-type while the other two to Neumann-type.

$$\begin{aligned} \theta(0,0) &= T_{w,P} - \frac{\alpha_{E,2s}}{\alpha_{E,2s}+\alpha_{W,2s}} T_{f,E,2s} - \frac{\alpha_{W,2s}}{\alpha_{E,2s}+\alpha_{W,2s}} T_{f,W,2s} \\ \theta(0,z_0) &= T_{w,P,t} - \frac{\alpha_{E,2s}}{\alpha_{E,2s}+\alpha_{W,2s}} T_{f,E,2s} - \frac{\alpha_{W,2s}}{\alpha_{E,2s}+\alpha_{W,2s}} T_{f,W,2s} \end{aligned} \tag{24}$$

$$\begin{aligned} \int_0^{z_0} k_w \left[\frac{\partial\theta(x,z)}{\partial x}\right]_{x=-0.5\delta x} s\,dz &= k_w \frac{T_{w,P,t} - T_{w,S,t} + T_{w,P} - T_{w,S}}{2\delta x} s z_0 \\ \int_0^{z_0} k_w \left[\frac{\partial\theta(x,z)}{\partial x}\right]_{x=+0.5\delta x} s\,dz &= k_w \frac{T_{w,N,t} - T_{w,P,t} + T_{w,N} - T_{w,P}}{2\delta x} s z_0 \end{aligned} \tag{25}$$

This system of equations can be solved. The first two conditions (24) involve the fin root temperatures while the last ones (25) ensure a coherent description of the thermal fluxes due to longitudinal conduction.

The proposed element makes use of different profile assumptions for calculating temperature and its derivative at the border. In this way, an additional advantage arises: since the conditions (25) force both side fluxes to be equal to FVM-like expressions, the continuity of fluxes at the border is satisfied and for whole extended surface too. As will be clearer in the following as regards the solution procedure, this feature is essential for SEWTLE technique because small discontinuities in thermal fluxes can prevent the convergence. Fortunately, the finite-volume description of EBS and the finite-element description of HBS by means of intrinsically conservative elements can be adopted together with SEWTLE.

The determined temperature profile can be used for calculating thermal fluxes through elementary surfaces (see Appendix).

6 Solution of system of discretization equations

The discretization equations for fluid (11) and for wall (17) have been expressed in terms of scalar variables. In order to adopt a matrix notation, the unknown fluid temperatures can be rearranged into vector $\mathbf{T_f}$, the upstream temperatures into vector $\mathbf{T^U}$ and the unknown wall temperatures into vector $\mathbf{T_w}$. The fluxes exchanged through elementary surfaces can be expressed as functions of the introduced vectors (see Appendix).

$$\Delta\Phi^{i,j,h-e}_{H-E-XBS} = [\mathbf{W^{i,j,h-e}_{H-E-XBS}}]\mathbf{T_w} + [\mathbf{F^{i,j,h-e}_{H-E-XBS}}]\mathbf{T_f} + [\mathbf{U^{i,j,h-e}_{H-E-XBS}}]\mathbf{T^U} \tag{26}$$

Introducing previous expressions into original discretization equations produces the cell contributions.

$$\begin{aligned} \forall i,j \quad &: \quad 1 \le i \le N_{fp} \quad ; \quad 1 \le j \le N_i \\ G_i c_p (T_i^j - T_i^{j-1}) \quad &= \quad [\mathbf{F1^{i,j}_f}]\mathbf{T_f} + [\mathbf{U1^{i,j}_f}]\mathbf{T^U} = [\mathbf{W^{i,j}_f}]\mathbf{T_w} + [\mathbf{F2^{i,j}_f}]\mathbf{T_f} + [\mathbf{U2^{i,j}_f}]\mathbf{T^U} \end{aligned} \tag{27}$$

According to FVM technique, the operator of Laplace can be expressed as a linear combination of unknown wall temperatures, arranged into vector $\mathbf{T_w}$.

$$\begin{aligned} \forall l \quad &: \quad 1 \le l \le N_w \\ \int_{\sigma^l_{EBS}} \nabla_2 \bullet (k_w \nabla_2 T_w) sdA \quad &= \quad [\mathbf{W1^l_w}]\mathbf{T_w} = [\mathbf{W2^l_w}]\mathbf{T_w} + [\mathbf{F^l_w}]\mathbf{T_f} + [\mathbf{U^l_w}]\mathbf{T^U} \end{aligned} \tag{28}$$

The cell contributions can be assembled into the final system of equations, which constitutes the skeleton of SEWTLE technique.

$$\textit{Step 1} \qquad \hat{\mathbf{T}}_\mathbf{f} = \{[\mathbf{F1_f}] - [\mathbf{F2_f}]\}^{-1} \left\{ [\mathbf{W_f}]\tilde{\mathbf{T}}_\mathbf{w} + [\mathbf{U2_f}]\mathbf{T^U} - [\mathbf{U1_f}]\mathbf{T^U} \right\} \tag{29}$$

$$\textit{Step 2} \qquad \hat{\mathbf{T}}_\mathbf{w} = \{[\mathbf{W1_w}] - [\mathbf{W2_w}]\}^{-1} \left\{ [\mathbf{F_w}]\hat{\mathbf{T}}_\mathbf{f} + [\mathbf{U_w}]\mathbf{T^U} \right\} \tag{30}$$

$$\textit{Step 3} \qquad \left| \frac{\Phi_H(\hat{\mathbf{T}}_\mathbf{f}, \tilde{\mathbf{T}}_\mathbf{w}) - \Phi_C(\hat{\mathbf{T}}_\mathbf{f}, \tilde{\mathbf{T}}_\mathbf{w})}{\Phi_H(\hat{\mathbf{T}}_\mathbf{f}, \tilde{\mathbf{T}}_\mathbf{w})} \right| \le Tol. \tag{31}$$

The notation $\tilde{T}$ indicates the values at the previous iteration, while $\hat{T}$ the new values. Φ_H and Φ_C are respectively the hot-side and cold-side approximations of exchanged thermal power. As previously discussed, the final step requires the adopted numerical schemes to be intrinsically conservative.

At generic step for resolution of wall field, an iterative procedure can be adopted for large heat exchangers: the simple Gauss-Seidel procedure is suggested. Since EBS is composed by surfaces linked together by transverse fins (Figure 1*a*, 1*b*), the Gauss-Seidel surface-by-surface method appears as the most natural choice. In some cases, the resolution system for generic EBS surface is large enough to suggest a further reduction by adopting the Gauss-Seidel line-by-line method which divides each surface into strips. In Figure 4 a comparison between the Gauss-Seidel methods is reported for a compact heat exchanger with microchannels. When a fully three-dimensional description is needed, the Gauss-Seidel line-by-line method is preferable because it drastically reduces the computation time required by SEWTLE, without increasing the number of iterations which must be properly managed if thermophysical properties depend on temperature.

7 Applications and discussion of results

7.1 Single fin

Some applications are discussed to illustrate the advantages of the proposed methodology.

Let us consider a thin plane which transfers heat to a surrounding fluid by convection and which is held at fixed temperature at the opposing bases. The temperature profile of the surrounding fluid depends on specific heat capacity and mass flow rate: for simplicity, a linear temperature profile has been assumed.

The geometric parameters and the operating conditions are reported in Table 1. This model problem is suitable to analyze the performances of a single smooth fin, according to classical theory of extended surface heat transfer [17]. The governing equations (22) have been numerically solved by means of FEM with surrounded triangular elements. The discretization has been refined in order to produce a mesh independent solution, which can be considered a reference for following comparisons (Figure 5*a*). Since the number of fins in a practical heat exchanger can be very high, a reduction of mesh density is needed. The simplest choice is to calculate convective thermal power by a linear temperature profile and then to subdivide it equally between fin roots (Figure 5*b*). The proposed methodology employs a shape function for temperature which takes into account the analytical solution of governing equations (Figure 5*c*). This strategy improves the accuracy in the calculation of convective heat transfer and allows properly estimating thermal fluxes at fin roots.

For the discussion of numerical results, some simplified analytical solutions can be useful. Let us suppose that $\alpha_{E,2s} = \alpha_{W,2s} = \alpha$ and $T_{f,E,2s} = T_{f,W,2s} = T_f(x)$. If the temperature rise for surrounding fluid can be neglected, the model problem is highly simplified and the following solution yields:

$$\theta(z) = \frac{\theta_1 - \theta_2 a}{1 - a^2} \exp\left(\sqrt{Bi}\,\frac{z}{z_0}\right) + \frac{\theta_2 a - \theta_1 a^2}{1 - a^2} \exp\left(-\sqrt{Bi}\,\frac{z}{z_0}\right) \tag{32}$$

where

$$\begin{aligned} \theta(z) &= T_w(z) - T_f \\ \theta_1 &= T_w(0) - T_f \\ \theta_2 &= T_w(z_0) - T_f \\ Bi &= 2\frac{\alpha z_0^2}{k_w s} \quad ; \quad a = \exp\sqrt{Bi} \end{aligned} \tag{33}$$

The ratio between the convective thermal power calculated by exact temperature profile and that by linear profile can be expressed in the following way:

$$\left(\frac{\Phi}{\Phi_V}\right)_{\Delta T_f = 0} = \frac{\int_0^{z_0}\int_0^{x_0} \alpha(T_w - T_f)dxdz}{\int_0^{z_0}\int_0^{x_0} \alpha(T_w^V - T_f)dxdz} = \frac{2}{\sqrt{Bi}}\frac{\exp\sqrt{Bi} - 1}{\exp\sqrt{Bi} + 1} < 1 \tag{34}$$

This ratio has been labeled as ideal law in Figure 6. The linear temperature profile adopted by FVM can be considered a good approximation at small Biot number. Otherwise the convective heat transfer forces to consider more complex shape functions. Tables 2, 3, 4 report the results of some numerical simulations performed by varying Biot number and temperature rise for surrounding fluid. The effect of temperature rise,

which determines the longitudinal conduction, increases the characteristic ratio if compared with ideal law.

$$\left(\frac{\Phi}{\Phi_V}\right)_{\Delta T_f=0} < \frac{\Phi}{\Phi_V} < 1 \tag{35}$$

Three simulations are shown in Figure 6. In all cases, the proposed conservative element reproduces very well the reference ($\Phi_E \approx \Phi$) and reveals its superiority at high Biot number in comparison with finite volume description which employs the same number of nodes ($\Phi_V > \Phi$).

The accuracy is not the only aspect to be considered. The thermal balance of generic fin can be expressed in the following way:

$$r + r^* = 1 \tag{36}$$

where r is the partition factor and r^* is its complement

$$r = \frac{\int_0^{x_0} k_w \left[\frac{\partial\theta(x,z)}{\partial z}\right]_{z=z_0} sdx}{\int_0^{z_0}\int_0^{x_0} \alpha(T_w - T_f)dxdz} \qquad r^* = -\frac{\int_0^{x_0} k_w \left[\frac{\partial\theta(x,z)}{\partial z}\right]_{z=0} sdx}{\int_0^{z_0}\int_0^{x_0} \alpha(T_w - T_f)dxdz} \tag{37}$$

When $r < 0$ or $r > 1$, a thermal bridge exists, i.e. one of fin roots is characterized by inverse thermal flux directed towards heated wall. Tables 2, 3, 4 report the partition factor calculated by proposed conservative FEM. Since FVM subdivides equally the convective thermal power between fin roots, it is characterized by a fixed value of partition factor $r = r^* = 0.5$. On the other hand, the proposed conservative element allows calculating the real distribution of thermal fluxes at any Biot number. Despite of classical FEM, the adopted boundary conditions for proposed element guarantee the continuity of thermal power, which can be employed as convergence check into SEWTLE technique.

7.2 Microchannel heat exchanger

The description of fins constitutes an essential step for analyzing the performances of whole heat exchanger. If a single fin is considered, there is no need to employ numerical schemes which are intrinsically conservative because only a local convergence criterion must be satisfied. On the other hand, the analysis of heat exchanger needs some iteration procedure and a global convergence criterion. Since the SEWTLE technique employs the transferred thermal power as convergence criterion, no source term for this quantity can be accepted in the discretized equations. As previously discussed, the proposed conservative elements satisfy this condition because they ensure exactly the thermal balance ($r + r^* = 1$), while the surrounded elements do it asymptotically ($r + r^* \to 1$).

A numerical code has been developed for fully-three dimensional description of cross-flow multi stream compact heat exchangers. The fins can be described by FVM or FEM with proposed conservative element as to investigate the most suitable technique and the effect on computational time. Let us consider a microchannel heat exchanger which cools a given mass flow rate of carbon dioxide by means of a water flow. The geometric parameters and the operating conditions are reported in Table 1. The microchannels for carbon dioxide are identified by vertical separating walls, called dividers, which represent a special kind of extended surfaces (Figure 1*b*). Table 5 reports the results of some numerical simulations performed by varying numerical scheme for extended surfaces and number of fins. The effect of numerical scheme depends on Biot number of considered surface. Since the Biot number for fins is quite high ($Bi = 7.7$) while the one for

dividers is negligible ($Bi = 0.1$), the calculated thermal power is mainly affected by numerical scheme selected to describe fins. For low numbers of fins ($N = 110 \div 550$), an increase of water-side extended surface increases the relative discrepancy between FVM and proposed FEM ($4.2 \div 7.9$ %). For high numbers of fins ($N = 550 \div 880$), an additional increase reduces the relative discrepancy ($7.9 \div 7.5$ %) because the performances of heat exchanger are less influenced by heat transfer surface. All the simulations show that the proposed FEM requires a greater computational time than FVM because the exponential function must be evaluated.

In Figure 7, the computational time and calculated thermal power for chosen methods are reported. This second application shows that the proposed FEM must be considered to describe every portion of extended surface characterized by high Biot numbers, also if this requires additional computational effort.

8 Conclusions

1. The mesh definition for calculation of complex heat exchangers has been extensively discussed. The grid generation and the cell discretization have been considered distinct processes according to numerical scheme chosen to improve the description.

2. The surrounded quadratic finite element has been modified in order to employ the analytical temperature profile for fin as shape function. The selected boundary conditions make the proposed finite element intrinsically conservative. This feature allows adopting the proposed element together with SEWTLE technique to describe finned surfaces because it does not compromise the convergence check based on exchanged thermal power.

3. At generic step for resolution of wall field, it has been demonstrated that the Gauss-Seidel line-by-line method is faster in the global iterative procedure realised by SEWTLE.

4. Finally, since FEM allows accurate temperature profile but increases computational time, it has been demonstrated that FEM must be applied only to finned surfaces characterized by high Biot numbers.

Acknowledgements

The author would like to thank Dr. Fabio Subba for his assistance in the revision of this article.

References

[1] E. S. Gaddis, D. B. Spalding, J. Taborek, Heat Exchanger Theory, in Begell House Inc. (ed.), *Heat Exchanger Design Handbook*, vol. I, chap. 1, Hemisphere, New York, 1989.

[2] W. M. Kays, A. L. London, *Compact Heat Exchangers*, McGraw-Hill, New York, 1984.

[3] P. Tochon, F. Michel, J. F. Fourmigué, P. Mercier, Advanced Numerical Methods for Compact Heat Exchanger Investigation, *Proc. of Compact Heat Exchangers Simposium*, Grenoble, France, vol. 1, pp. 57-64, 2002.

[4] P. Geiser, V. Kottke, Numerical Simulations of Temperature, Heat Transfer and Heat Flux in Flat and Finned Tube Heat Exchangers, *Proc. of Compact Heat Exchangers Simposium*, Grenoble, France, pp. 157-162, 2002.

[5] J. P. Chiou, The Effect of Longitudinal Heat Conduction on Crossflow Heat Exchanger, *Trans. ASME, J. Heat Transfer*, vol. 100, pp. 346-351, 1978.

[6] Ch. Ranganayakulu, K. N. Seetharamu, K. V. Sreevatsan, The Effects of Longitudinal Conduction in Compact Plate-Fin and Tube-Fin Heat Exchangers Using a Finite-Element Method, *Int. J. Heat Mass Transfer*, vol. 40, no. 6, pp. 1261-1277, 1997.

[7] Ch. Ranganayakulu, K. N. Seetharamu, K. V. Sreevatsan, The Effects of Inlet Fluid Flow Nonuniformity on Thermal Performance and Pressure Drops in Crossflow Plate-Fin Compact Heat Exchangers, *Int. J. Heat Mass Transfer*, vol. 40, no. 1, pp. 27-38, 1997.

[8] J. P. Chiou, The Advancement of Compact Heat Exchanger Theory Considering the Effects of Longitudinal Heat Conduction and Flow Nonuniformity, *Symp. Compact Heat Exchangers-History, ASME*, pp. 101-105, 1980.

[9] Ch. Ranganayakulu, K. N. Seetharamu, The Combined Effects of Wall Longitudinal Heat Conduction, Inlet Fluid Flow Nonuniformity and Temperature Nonuniformity in Compact Tube-Fin Heat Exchangers: a Finite Element Method, *Int. J. Heat Mass Transfer*, vol. 42, pp. 263-273, 1999.

[10] J. M. Corberán, P. F. De Córdoba, J. Gonzálvez, F. Alias, Semiexplicit Method for Wall Temperature Linked Equations (SEWTLE): a General Finite-Volume Technique for the Calculation of Complex Heat Exchangers, *Numerical Heat Transfer: Part. B*, vol. 40, pp. 37-59, 2001.

[11] J. M. Yin, C. W. Bullard, P. S. Hrnjak, R-744 Gas Cooler Model Development and Validation, *Int. J. of Refrigeration*, vol. 24, no. 6, pp. 652-659, 2002.

[12] R. Romero-Méndez, M. Sen, K. T. Yang, R. L. McLain, Effect of Tube-To-Tube Conduction on Plate-Fin and Tube Heat Exchanger Performance, *Int. J. Heat Mass Transfer*, vol. 40, no. 16, pp. 3909-3916, 1997.

[13] J. L. Lage, Tube-To-Tube Heat Transfer Degradation Effect on Finned-Tube Heat Exchangers, *Numerical Heat Transfer: Part A*, vol. 39, pp. 321-337, 2001.

[14] S. V. Patankar, *Numerical Heat Transfer and Fluid Flow*, Hemisphere, New York, 1980.

[15] L. J. Segerlind, *Applied finite analysis*, Wiley, New York, 1984.

[16] M. L. Krasnov, G. I. Makarenko, A. I. Kiselev, *Calculus of variations*, MIR Editions, Moscow, 1984.

[17] B. S. V. Prasad, Fin Efficiency and Mechanisms of Heat Exchange Through Fins in Multi-Stream Plate-Fin Heat Exchangers: Formulation, *Int. J. Heat Mass Transfer*, vol. 39, no. 2, pp. 419-428, 1996.

Appendix

The algebraic equations due to discretization process have been expressed by means of thermal fluxes exchanged through elementary surfaces.

Let us consider the generic fluid cell (i, j) shown in Figure $2d$ and suppose that $\alpha_{E,2s} = \alpha_{W,2s} = \alpha$ and $T_{f,E,2s} = T_{f,W,2s} = T_f$. The temperature profile defined by variational principle must be calculated firstly by conditions (24) and (25).

$$\begin{cases} C_1 + C_2 + C_3 + C_4 = T_{w,P} - T_f \\ C_1 + C_2 + C_3 a + \frac{1}{a} C_4 = T_{w,P,t} - T_f \\ C_1 \frac{1}{\sqrt{b}} - C_2 \sqrt{b} = \frac{z_0}{2\delta x \sqrt{Bi}} \left(T_{w,P,t} - T_{w,S,t} + T_{w,P} - T_{w,S} \right) \\ C_1 \sqrt{b} - C_2 \frac{1}{\sqrt{b}} = \frac{z_0}{2\delta x \sqrt{Bi}} \left(T_{w,N,t} - T_{w,P,t} + T_{w,N} - T_{w,P} \right) \end{cases} \tag{38}$$

where

$$a = \exp\left(\sqrt{Bi}\right) \quad ; \quad b = \exp\left(\sqrt{Bi}\, \frac{\delta x}{z_0}\right)$$

This system of equations allows to determine the generic constants C_i and to identify the element temperature profile. The constants C_i are linear functions of unknown fluid temperatures $\mathbf{T_f}$, upstream temperatures $\mathbf{T^U}$ and unknown wall temperatures $\mathbf{T_w}$. The convective thermal fluxes for HBS elementary surfaces can be expressed as:

$$\Delta\Phi_{HBS}^{i,j,2} = \Delta\Phi_{HBS}^{i,j,3} = \int_0^{z_0} \int_{-0.5\delta x}^{0} \alpha\theta(x,z) dx dz \tag{39}$$

$$\Delta\Phi_{HBS}^{i,j,1} = \Delta\Phi_{HBS}^{i,j,4} = \int_0^{z_0} \int_{0}^{0.5\delta x} \alpha\theta(x,z) dx dz \tag{40}$$

Introducing the element temperature profile, the previous integrals can be evaluated.

$$\Delta\Phi_{HBS}^{i,j,2-3} = \alpha \frac{z_0^2}{\sqrt{Bi}} \quad \left[\left(\sqrt{b} - 1\right) C_1 + \left(1 - \frac{1}{\sqrt{b}}\right) C_2 + \frac{1}{2}\frac{\delta x}{z_0} (a-1) C_3 + \frac{1}{2}\frac{\delta x}{z_0} \left(1 - \frac{1}{a}\right) C_4 \right] \tag{41}$$

$$\Delta\Phi_{HBS}^{i,j,1-4} = \alpha \frac{z_0^2}{\sqrt{Bi}} \quad \left[\left(1 - \frac{1}{\sqrt{b}}\right) C_1 + \left(\sqrt{b} - 1\right) C_2 + \frac{1}{2}\frac{\delta x}{z_0} (a-1) C_3 + \frac{1}{2}\frac{\delta x}{z_0} \left(1 - \frac{1}{a}\right) C_4 \right] \tag{42}$$

The conductive thermal fluxes for XBS elementary surfaces can be expressed in the same way.

$$\Delta\Phi_{XBS}^{i,j,1} = \Delta\Phi_{XBS}^{i,j,4} = \int_0^{0.5\delta x} \frac{k_w s}{2} \left[\frac{\partial\theta(x,z)}{\partial z}\right]_{z=0} dx \tag{43}$$

$$\Delta\Phi_{XBS}^{i,j,2} = \Delta\Phi_{XBS}^{i,j,3} = \int_{-0.5\delta x}^{0} \frac{k_w s}{2} \left[\frac{\partial\theta(x,z)}{\partial z}\right]_{z=0} dx \tag{44}$$

$$\Delta\Phi_{XBS}^{i,j,5} = \Delta\Phi_{XBS}^{i,j,8} = -\int_0^{0.5\delta x} \frac{k_w s}{2} \left[\frac{\partial\theta(x,z)}{\partial z}\right]_{z=z_0} dx \tag{45}$$

$$\Delta\Phi_{XBS}^{i,j,6} = \Delta\Phi_{XBS}^{i,j,7} = -\int_{-0.5\delta x}^{0} \frac{k_w s}{2} \left[\frac{\partial\theta(x,z)}{\partial z}\right]_{z=z_0} dx \tag{46}$$

Introducing the element temperature profile, the previous integral can be evaluated.

$$\Delta\Phi_{XBS}^{i,j,1-2-3-4} = \frac{k_w s}{4}\sqrt{Bi}\,\frac{\delta x}{z_0}\,(C_3 - C_4) \tag{47}$$

$$\Delta\Phi_{XBS}^{i,j,5-6-7-8} = \frac{k_w s}{4}\sqrt{Bi}\,\frac{\delta x}{z_0}\left(aC_3 - \frac{1}{a}C_4\right) \tag{48}$$

Since previous expressions (41, 42, 47, 48) are linear functions of constants C_i which are linear functions of grid temperatures, the thermal fluxes $\Delta\Phi_{HBS}^{i,j,h}$ and $\Delta\Phi_{XBS}^{i,j,e}$ can be considered as linear functions of grid temperatures too. On the other hand, the fluxes $\Delta\Phi_{EBS}^{i,j,e}$ exchanged through EBS elementary surfaces can be easily espressed in the same way by means of FVM.

Therefore, the following expression yields for any elementary surface.

$$\Delta\Phi_{H-E-XBS}^{i,j,h-e} = [\mathbf{W}_{\mathbf{H-E-XBS}}^{\mathbf{i,j,h-e}}]\mathbf{T_w} + [\mathbf{F}_{\mathbf{H-E-XBS}}^{\mathbf{i,j,h-e}}]\mathbf{T_f} + [\mathbf{U}_{\mathbf{H-E-XBS}}^{\mathbf{i,j,h-e}}]\mathbf{T^U} \tag{49}$$

List of Tables

Table 1: Geometric parameters and operating conditions for considered applications.

	Geometric parameters		Operating conditions	
Application 1	Fin length (mm)	16.0	Temp. top root (K)	390
	Fin height (mm)	3.2-9.0	Temp. bottom root (K)	340
	Fin thichness (mm)	0.1	Temp. fluid inlet (K)	300
			Temp. rise (K)	0-33
			Conductivity (W/mK)	200
Application 2	Plate length (mm)	250.0	Mass flow CO_2 (g/s)	43.0
	Plate width (mm)	16.5	Temp. inlet CO_2 (K)	351.4
	Plate height (mm)	1.65	Pressure CO_2 (bar)	76.6
	Channel number	11	Mass flow H_2O (g/s)	181.1
	Channel diam. (mm)	0.79	Temp. inlet H_2O (K)	300.0
	Fin height (mm)	8.8	Conductivity (W/mK)	200
	Fin thickness (mm)	0.1		
	Num. of plates	12		
	Num. of passes	3		
	Plates in 1th pass	5		
	Plates in 2nd pass	4		
	Plates in 3rd pass	3		

Table 2: Results of calculations about single fin. The linear temperature profile has been assumed for fluid and the global temperature rise is $\Delta T_f = 0.0\ K$.

			Thermal Power (W)					
				Model (P)			$\left(\frac{P-Q}{Q}\right)$ x 100	
$h\ (mm)$	$\alpha\ (W/m^2K)$	Bi	Ref.(Q)	FVM	FEM	r	FVM	FEM
9.0	50	0.41	0.623	0.644	0.623	2.529	+3.37	+0.00
9.0	500	4.05	4.890	6.435	4.887	0.829	+31.60	-0.06
9.0	1000	8.10	8.060	12.870	8.051	0.743	+59.68	-0.11
9.0	1500	12.15	10.433	19.305	10.418	0.717	+85.04	-0.14
9.0	2000	16.20	12.364	25.740	12.341	0.707	+108.19	-0.19
8.4	2000	14.11	12.222	24.024	12.206	0.711	+96.56	-0.13
7.1	2000	10.08	11.781	20.306	11.764	0.727	+72.36	-0.14
5.4	2000	5.83	10.696	15.444	10.692	0.775	+44.39	-0.04
3.2	2000	2.05	7.858	9.152	7.855	1.010	+16.47	-0.04

Table 3: Results of calculations about single fin. The linear temperature profile has been assumed for fluid and the global temperature rise is $\Delta T_f = 16.5\ K$.

			Thermal Power (W)					
				Model (P)			$\left(\frac{P-Q}{Q}\right)$ x 100	
h (mm)	α (W/m^2K)	Bi	Ref.(Q)	FVM	FEM	r	FVM	FEM
9.0	50	0.41	0.544	0.562	0.544	2.824	+3.31	+0.00
9.0	500	4.05	4.274	5.618	4.267	0.877	+31.45	-0.16
9.0	1000	8.10	7.045	11.237	7.029	0.778	+59.50	-0.23
9.0	1500	12.15	9.121	16.855	9.096	0.749	+84.79	-0.27
9.0	2000	16.20	10.811	22.473	10.775	0.737	+107.87	-0.33
8.4	2000	14.11	10.676	20.975	10.657	0.742	+96.47	-0.18
7.1	2000	10.08	10.298	17.729	10.271	0.760	+72.16	-0.26
5.4	2000	5.83	9.359	13.484	9.335	0.815	+44.08	-0.26
3.2	2000	2.05	6.866	7.990	6.858	1.084	+16.37	-0.12

Table 4: Results of calculations about single fin. The linear temperature profile has been assumed for fluid and the global temperature rise is $\Delta T_f = 33.0\ K$.

			Thermal Power (W)					
				Model (P)			$\left(\frac{P-Q}{Q}\right)$ x 100	
h (mm)	α (W/m^2K)	Bi	Ref.(Q)	FVM	FEM	r	FVM	FEM
9.0	50	0.41	0.465	0.480	0.465	3.219	+3.23	+0.00
9.0	500	4.05	3.657	4.802	3.647	0.941	+31.31	-0.27
9.0	1000	8.10	6.030	9.603	6.008	0.825	+59.25	-0.37
9.0	1500	12.15	7.809	14.405	7.774	0.791	+84.47	-0.45
9.0	2000	16.20	9.258	19.206	9.209	0.777	+107.45	-0.53
8.4	2000	14.11	9.117	17.926	9.108	0.783	+96.62	-0.10
7.1	2000	10.08	8.816	15.151	8.778	0.805	+71.86	-0.43
5.4	2000	5.83	8.011	11.524	7.978	0.869	+43.85	-0.41
3.2	2000	2.05	5.875	6.829	5.861	1.183	+16.24	-0.24

Table 5: Results of calculations about microchannel heat exchanger.

N. fins		Fin model / Divider model				$\left(\frac{P-Q}{Q}\right)$ x 100
		$V/V(P)$	V/E	E/V	$E/E(Q)$	
110	N. iter.	317	317	335	330	-3.94
	Time (s)	30	32	34	34	-11.76
	Power (W)	2402	2402	2305	2305	+4.21
220	N. iter.	292	293	318	318	-8.18
	Time (s)	54	57	62	66	-18.18
	Power (W)	2624	2624	2469	2469	+6.28
330	N. iter.	282	277	313	310	-9.03
	Time (s)	76	79	90	95	-20.00
	Power (W)	2791	2790	2604	2604	+7.18
440	N. iter.	273	272	318	311	-12.22
	Time (s)	96	101	119	122	-21.31
	Power (W)	2923	2923	2717	2717	+7.58
550	N. iter.	277	274	325	319	-13.17
	Time (s)	119	125	151	155	-23.23
	Power (W)	3033	3033	2812	2812	+7.86
660	N. iter.	287	280	336	332	-13.55
	Time (s)	149	150	185	189	-21.16
	Power (W)	3123	3123	2897	2896	+7.84
770	N. iter.	299	292	351	346	-13.58
	Time (s)	175	181	223	230	-23.91
	Power (W)	3200	3200	2971	2971	+7.71
880	N. iter.	313	306	376	366	-14.48
	Time (s)	208	214	270	277	-24.91
	Power (W)	3266	3266	3037	3037	+7.54

List of Figures

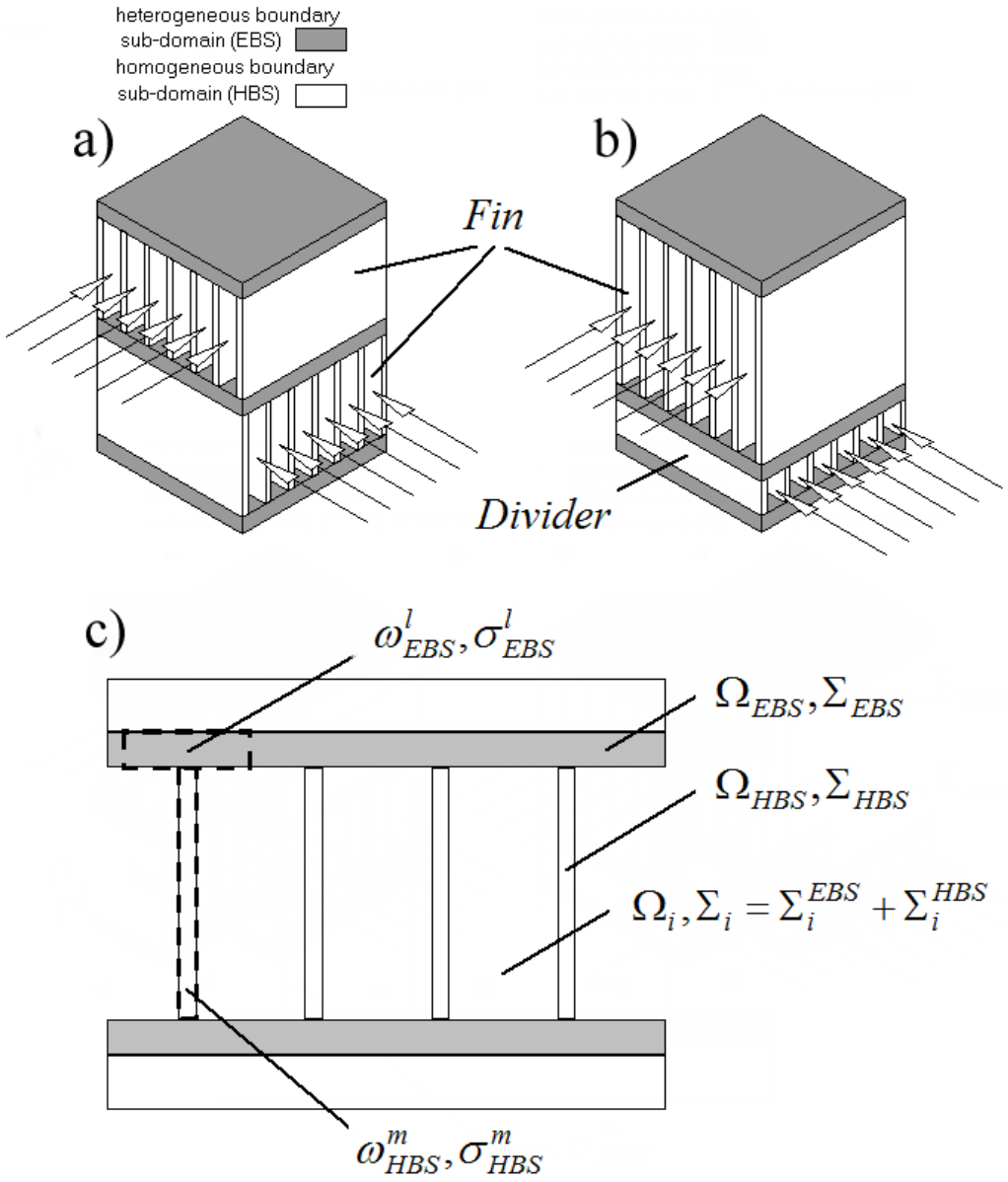

Figure 1: Visualization of conventional terminology: difference between EBS and HBS, between fins and dividers and between global calculation domains Ω and discretized domains ω. (a) Crossflow plate-fin heat exchanger. (b) Crossflow plate-fin heat exchanger with microchannels. (c) Considered discretization.

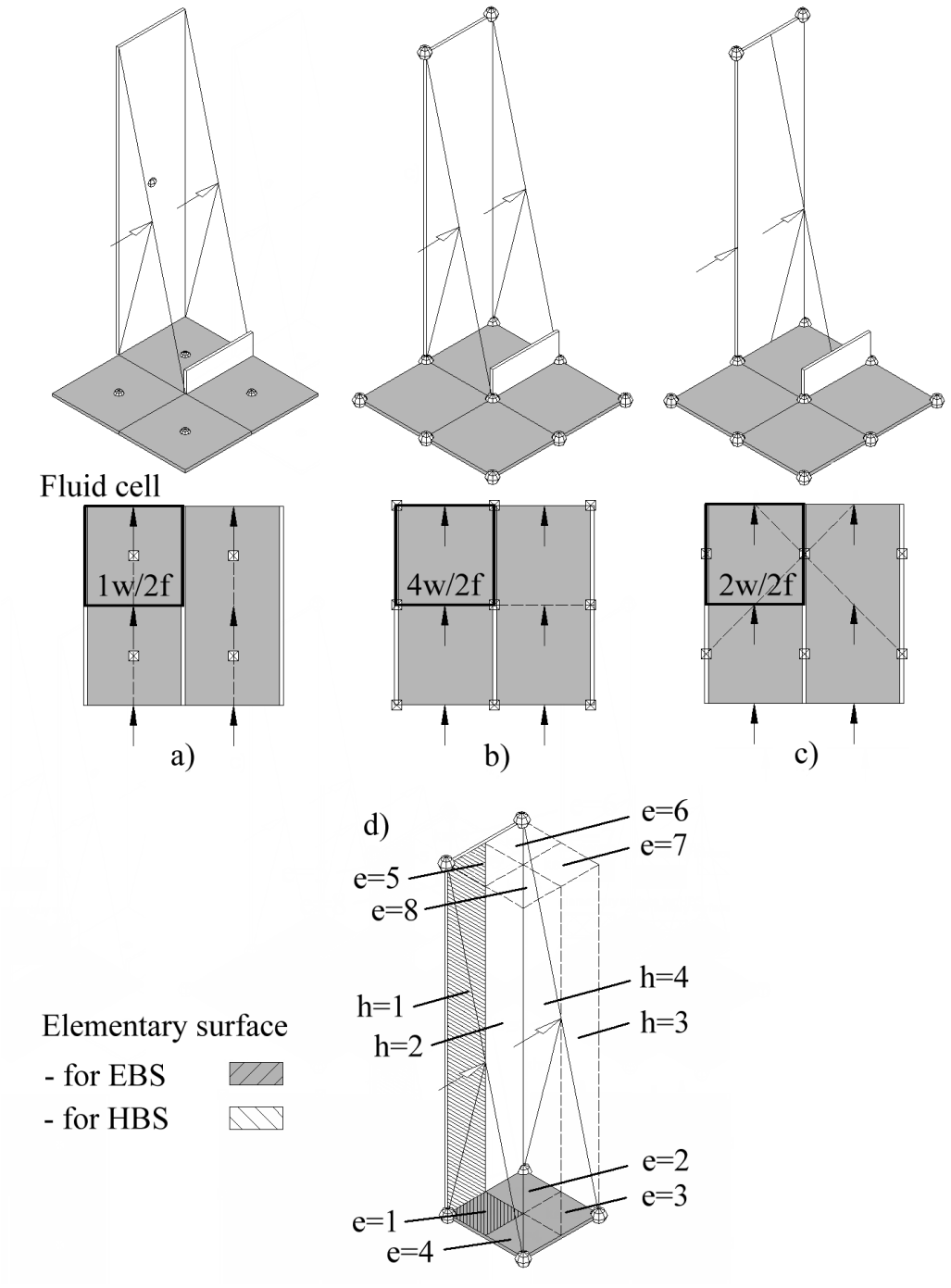

Figure 2: Relative arrangement between wall grid (square markers) and fluid grid (arrow markers): (a) longitudinal configuration; (b) transverse configuration and (c) diagonal configuration. All configurations show the projection of fluid cell adopted in calculations and the ratio between wall points and fluid ones (w/f). (d) Numeration of elementary surfaces for fluid cell with transverse configuration.

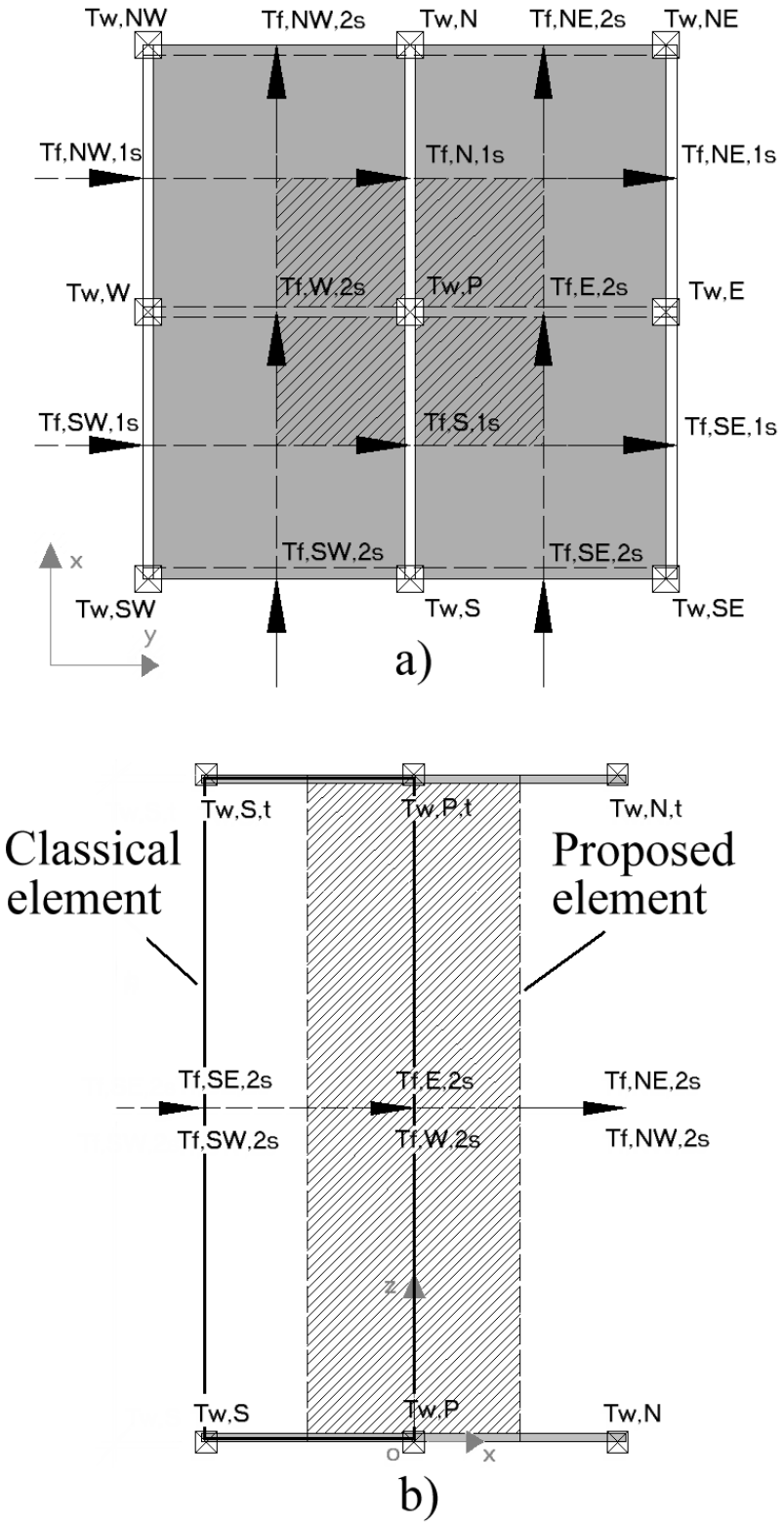

Figure 3: Schematic view of the EBS cell (a) and HBS cell (b) surrounded by fluid paths involved in the convective heat transfer. In the HBS cell, the comparison between the proposed element and classical one is also reported.

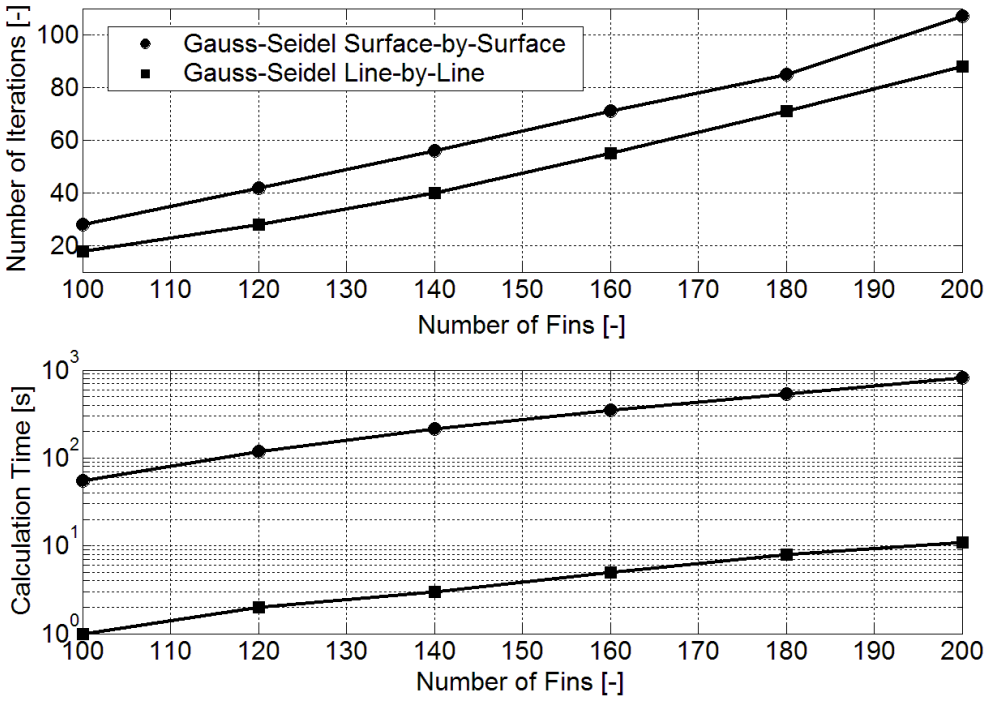

Figure 4: Comparison between GSSS (Gauss-Seidel surface-by-surface) and GSLL (Gauss-Seidel line-by-line) method within a SEWTLE technique with control tolerance of 0.1 % on thermal power for a compact heat exchanger with microchannels.

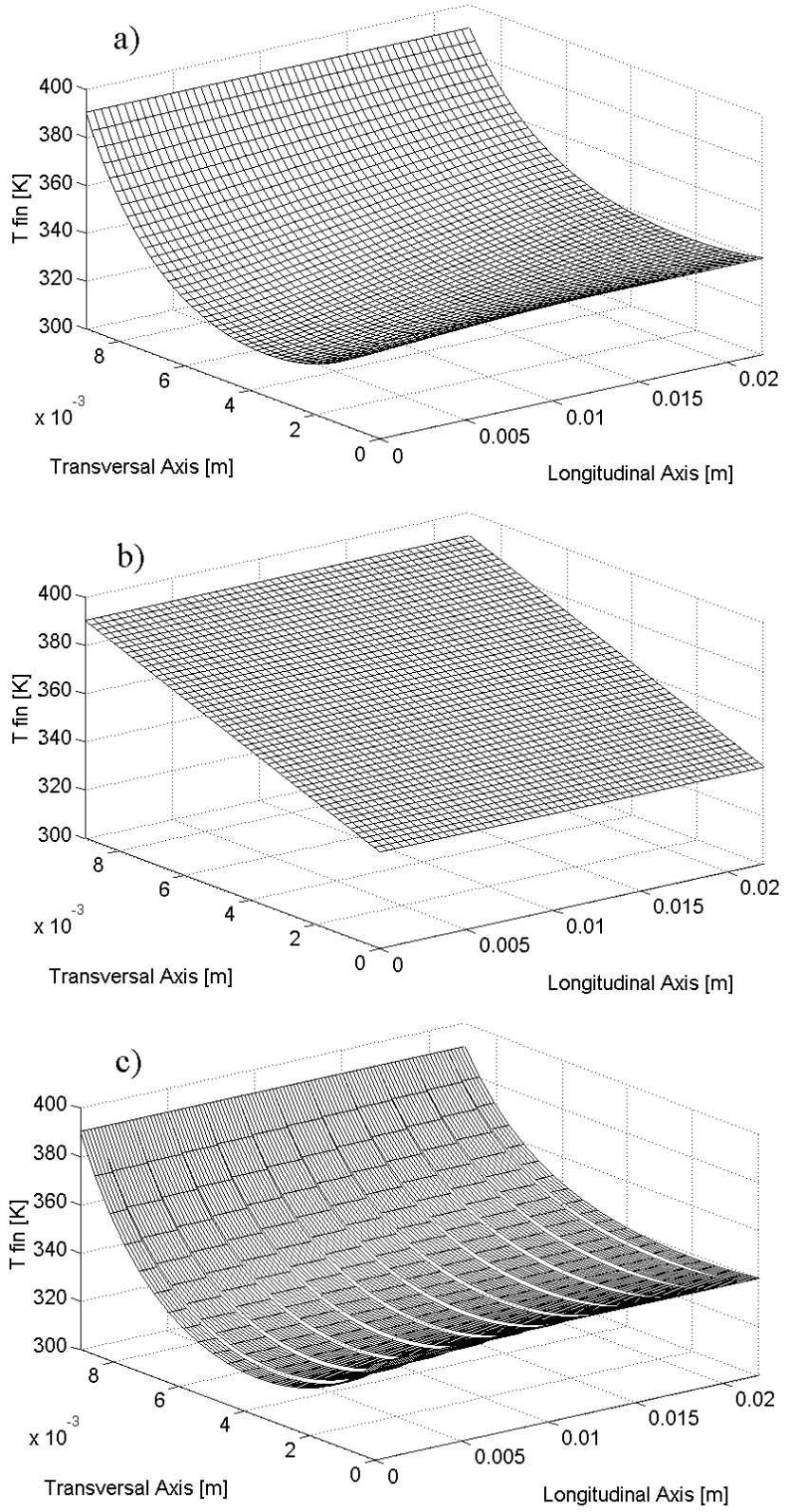

Figure 5: Fin temperature profiles described by different models: (a) high resolution FEM assumed as reference; (b) FVM description based on temperatures at fin roots and (c) intrinsically conservative FEM based on temperatures at fin roots.

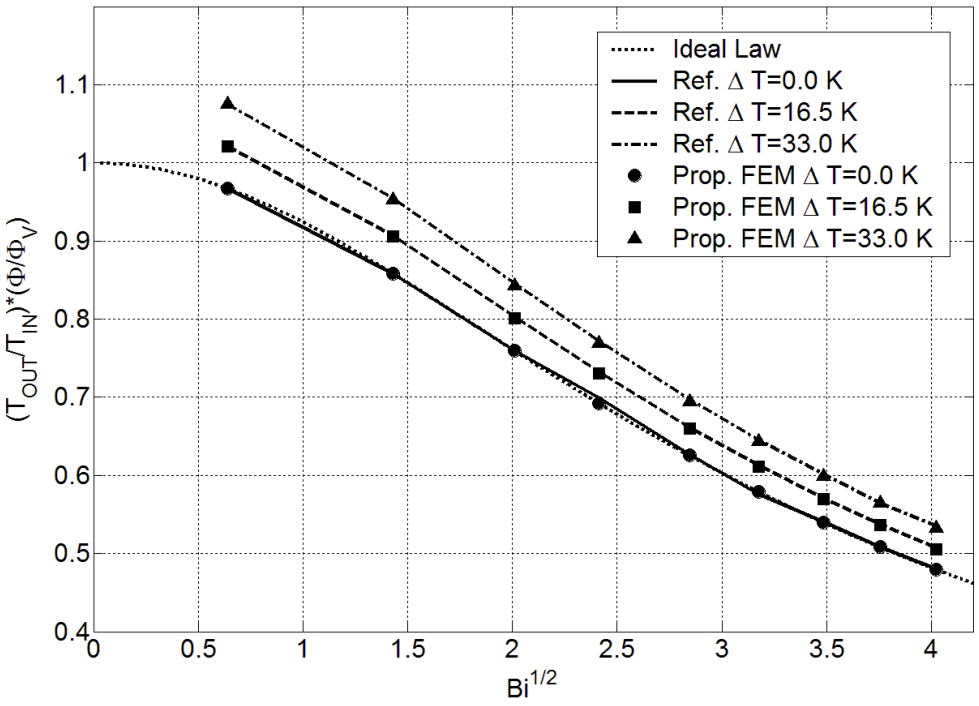

Figure 6: Results of calculations about single fin. The thermal powers calculated by the proposed methodology and the reference are reported for different temperature rises of fluid. The ratio T_{OUT}/T_{IN} helps to distinguish the results of simulations.

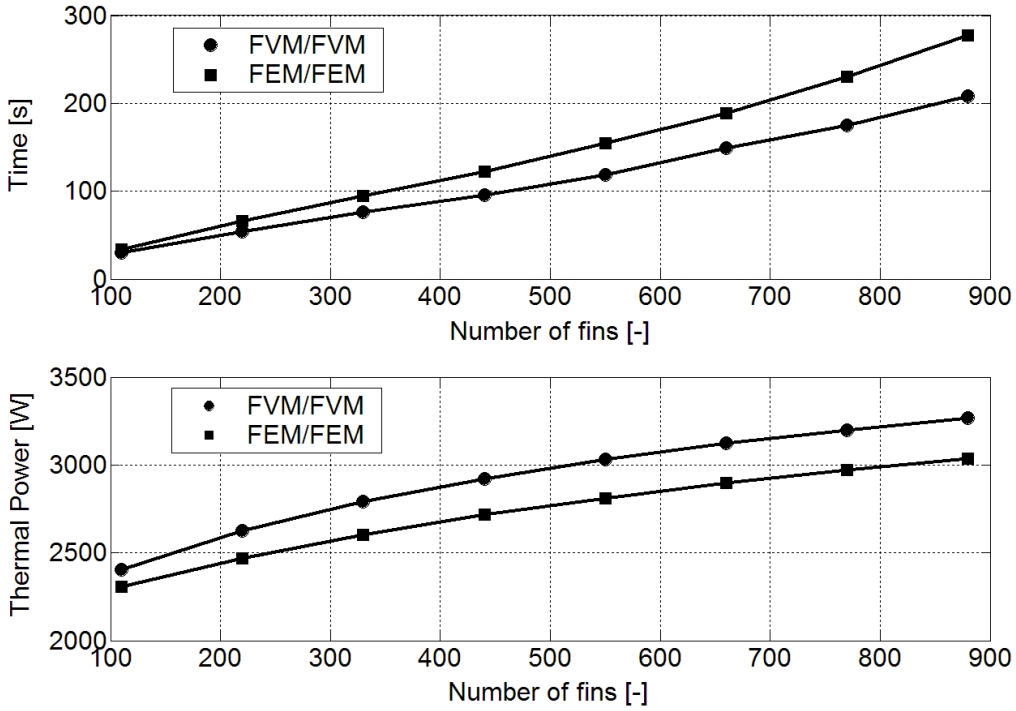

Figure 7: Results of calculations about microchannel heat exchanger. The FVM requires less calculation time but underestimates the exchanged thermal power.